Uncertainty estimation for turbulence models in aerospace applications

By A. A. Mishra AND G. Iaccarino

1. Introduction

Turbulent flows are found in manifold applications of aerospace interest. While computationally intensive approaches like Direct Numerical Simulations (DNS) and Large Eddy Simulations (LES) offer high degrees of fidelity, their computational cost is too high to enable their use as a pragmatic design tool. Consequently, a vast majority of CFD studies of aerospace systems utilize simpler Reynolds Averaged Navier-Stokes (RANS) closures to account for the effects of turbulence. Typically linear two-equation $k-\epsilon$ or $k-\omega$ closures are used in industrial applications (Georgiadis *et al.* 2006*b*).

In spite of their wide spread use, RANS-based models suffer from an inherent structural inability to replicate fundamental turbulence processes. Due to the assumptions and simplifications invoked in model formulation, RANS models are limited with respect to the features of turbulence they can represent and the fidelity with which they can represent these features.

To aid the establishment of RANS simulations as reliable tools for aerospace applications, in addition to improved predictive fidelity, we require explicit quantification of the uncertainty in model predictions. Recently, a physics-based framework to estimate the model inadequacy in turbulence closures has been developed (Emory *et al.* 2013; Iaccarino *et al.* 2017). This utilizes sequential perturbations injected into the modeled Reynolds stress eigenvalues, eigenvectors and the turbulent kinetic energy. The perturbations to the Reynolds stress eigenvalues quantify the variability in the componentiality of the turbulent flow field. The eigenvector perturbations assess the volatility in the production mechanism. Finally, the turbulent kinetic energy perturbations estimate the incertitude in the modeling of the triple correlation terms. Using these sequential perturbations, this framework ascertains the uncertainty due to limitations in model form. This framework has been successfully applied to a variety of canonical flows and benchmark cases (Emory *et al.* 2013, 2011; Mishra & Iaccarino 2016; Xiao *et al.* 2016; Wu *et al.* 2015; Mishra *et al.* 2016; Gorlé *et al.* 2012).

In this investigation, we utilize this uncertainty estimation procedure to quantify the discrepancy between RANS predictions and high fidelity data for high-speed, turbulent jets in the exhaust of aircraft. The efficacy of the eigenspace perturbation technique is investigated for a variety of different nozzle geometries, at super- and sub-sonic conditions, for both heated and cooled jets and for a range of Quantities of Interest.

After a brief overview in Section 1, Section 2 motivates the importance of reliable predictions for aircraft nozzle jets and introduces the mathematical details of the Eigenspace Perturbation framework. Section 3 delineates the results from the application of this uncertainty estimation framework to sub- and super-sonic jets. Herein we focus on exhibiting the prediction intervals from the procedure and contrasting it to the higher fidelity data along with the unperturbed RANS results. Section 4 summarizes the results and outlines future steps.

2. Mathematical details

Most modern aircraft are powered by gas turbine engines. The nozzle is a key component of the aircraft engine as the nozzle transforms it from a gas turbine to a jet engine. Energy available in the gas turbine exhaust is converted into a high-speed jet by the contoured nozzle, producing thrust that propels the aircraft.

In this context, reliable predictions of turbulent jets exhausting from contoured aircraft nozzles are critical for a multitude of applications. Such predictions are essential to calculate key engine operation parameters such as thrust for diverse designs and operating conditions. Furthermore, with the introduction of stringent guidelines on aircraft noise, there has been an impetus to demonstrate improved predictions for exhaust jets. There is a focused effort to experiment with new designs for such nozzles, incorporating chevrons, bevels, tabs, lobed mixers, etc (Georgiadis *et al.* 2006*a*). The development of such concepts can be enhanced through the use of reliable CFD simulations. The efflux of the aircraft nozzle involves interaction of the jet and ambient, affected by complicated nozzle geometries, significant compressibility effects, imperfect expansion, and the interaction of high temperature streams. These complications pose challenges to RANS closures. For instance, we focus upon the mixing between the jet flow and the ambient. Close to the jet exit, RANS models predict a significantly lower rate of initial jet mixing as contrasted against high-fidelity data (Georgiadis *et al.* 2006*b*; Koch *et al.* 2002; Georgiadis *et al.* 2006*a*; Engblom *et al.* 2004). Contrastingly, farther downstream of the jet potential core, RANS models predict the far-field mixing rate to become significantly higher than is observed in experiments (Dembowski & Georgiadis 2002; Georgiadis *et al.* 2006*b*,*a*). Similarly, the fidelity of RANS predictions is highly inconsistent, having higher fidelity for cold jets than heated, for axisymmetric than non-axisymmetric geometries, varying significantly over different Quantities of Interest (QoIs), etc. The flow in exhaust jets is challenging to predict correctly with model forms or coefficients determined from other flows Hussein *et al.* (1994). Furthermore, there is significant incertitude regarding the turbulent kinetic energy budget in such flows due to the presence of large scale instabilities and mixing, hampering the development of models with higher fidelity Taulbee *et al.* (1987). Additionally, the development of these flows is extremely sensitive to ancillary parameters such as the nozzle contour, minute details of the ambient flow Hussein *et al.* (1994); Schneider (1985), etc. To address these drawbacks, there have been many efforts to improve the performance of RANS models for turbulent jets. For instance, Thies & Tam (1996) have developed a $k-\epsilon$ closure specifically calibrated for jet flows. In a similar vein, the Sarkar correction for compressibility (Sarkar *et al.* 1991) and the round jet correction (Pope (1978)) have been incorporated. Additionally, Tam *et al.* (2004) have specifically developed corrections for heated jets. However, the improvements due to these have been but incremental. RANS closures still face issues of accuracy, robustness and reliability.

Turbulence models are constitutive relations attempting to relate unknown quantities (including higher-order statistical moments) to local, low-order flow quantities using simplifying assumptions. In this context, the goal of Reynolds Averaged Navier Stokes closures is to determine the Reynolds stress tensor in terms of mean flow quantities that are directly computable. To this end, RANS models utilize the conceptualization of an isotropic eddy viscosity and the modeling of turbulence processes via the gradient diffusion hypothesis.

Utilizing the eigenvalue decomposition, the symmetric Reynolds stress tensor, $R_{ij} =$

$\langle u_i u_j \rangle$, is

$$R_{ij} = 2k\left(\frac{\delta_{ij}}{3} + v_{in}\Lambda_{nl}v_{lj}\right) \tag{2.1}$$

wherein k, denotes the turbulent kinetic energy, v represents the eigenvector matrix, and, Λ, the diagonal matrix of eigenvalues of the Reynolds stress tensor. The tensors v and Λ are ordered such that $\lambda_1 \geq \lambda_2 \geq \lambda_3$. The amplitude, the shape and the orientation of the Reynolds stress are explicitly represented by k, λ_i and v_{ij}, respectively. The objective of this study is to determine the possible range of Reynolds stresses for a specific flow, given a set of modeling assumptions. We apply a framework to perturb the eigenvalues and eigenvectors in Eq. (1). The perturbations are injected directly into the modeled Reynolds stress, expressed as

$$R^*_{ij} = 2k^*\left(\frac{\delta_{ij}}{3} + v^*_{in}\Lambda^*_{nl}v^*_{lj}\right) \tag{2.2}$$

wherein * represents the perturbed quantities. The perturbations to the eigenvalues, Λ, correspond to varying the componentiality of the flow, or equivalently, the shape of the Reynolds stress ellipsoid. These are defined through the coordinates in the barycentric map, x, via $\lambda^*_i = B^{-1}\mathbf{x}^*$, where perturbed quantities are starred and B is the transformation from the eigenvalue space to the barycentric triangle (Emory *et al.* 2013). The projection of the eigenvalue perturbation in the barycentric map has both a direction and a magnitude. Considering the extreme states of Reynolds stress componentiality, we consider perturbation alignments to the three vertices of the triangle: x_{1C}, x_{2C}, x_{3C} representing the limiting states of turbulence anisotropy. The magnitude of the perturbation in the barycentric triangle is represented by $\Delta_B \in [0, 1]$. Thus, the perturbed barycentric coordinates, $\mathbf{x}^*$, are given by: $\mathbf{x}^* = x + \Delta_B(\mathbf{x}^{(t)} - \mathbf{x})$, where x^t denotes the target vertex (representing one of the one-, two- or three-component limiting states) and x is the model prediction. Instead of relying on a user-defined magnitude for Δ_B , we set $\Delta_B = 1.0$ so that the three limiting states are considered.

The perturbations to the eigenvectors, v, correspond to varying the alignment of the Reynolds stress ellipsoid. To guide these, we focus on the production mechanism, $\mathcal{P} = -R_{ij}\partial U_i/\partial x_j$. The eigenvector perturbations seek to modulate turbulence production by varying the Frobenius inner product $\langle A, R\rangle = tr(AR)$, where A is the mean gradient and R is the Reynolds stress tensor. For the purposes of bounding all permissible dynamics, we seek the extremal values of this inner product. In the coordinate system defined by the eigenvectors of the rate of strain tensor, the critical alignments of the Reynolds stress eigenvectors are given by

$$v_{max} = \begin{bmatrix} 1 & 0 & 0 \\ 0 & 1 & 0 \\ 0 & 0 & 1 \end{bmatrix}, \quad v_{min} = \begin{bmatrix} 0 & 0 & 1 \\ 0 & 1 & 0 \\ 1 & 0 & 0 \end{bmatrix}. \tag{2.3}$$

The corresponding ranges of the inner products therefrom are $[\lambda_1\gamma_3 + \lambda_2\gamma_2 + \lambda_3\gamma_1, \lambda_1\gamma_1 + \lambda_2\gamma_2 + \lambda_3\gamma_3]$, where $\gamma_1 \geq \gamma_2 \geq \gamma_3$ are the eigenvalues of the symmetric component of A.

This eigenspace perturbation framework gives us 5 distinct extremal states of the Reynolds stress tensor. These correspond to 3 extremal states of the componentiality $(1C, 2C, 3C)$ and 2 extremal alignments of the Reynolds stress eigenvectors, (v_{min}, v_{max}). Thus, for complete uncertainty bounds on flow evolution, we need a maximal set of only 5 RANS simulations.

This methodology can be applied to any RANS-based model, including second moment

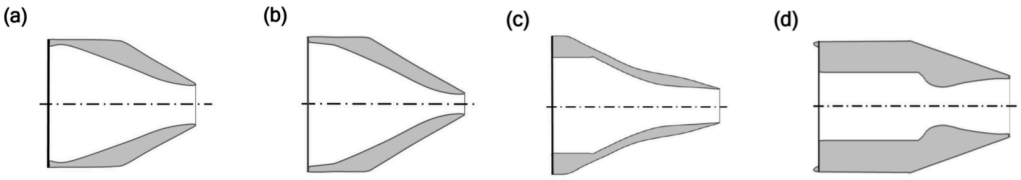

FIGURE 1. Schematic detailing the nozzle geometries investigated: (a) NASA Acoustic Reference Nozzle 1 (ARN1), (b) NASA Acoustic Reference Nozzle 2 (ARN2), (c) Small Metal Chevron (SMC000) nozzle, (d) Eggers Nozzle.

closures. For the purposes of this investigation, we restrict ourselves to the SST model of Menter (1994). The results presented hereon must be interpreted as the range of possible flow evolutions corresponding to the Reynolds stress eigenspace perturbations, that are constrained by the SST model. Results corresponding to the Shear Stress Transport model bereft of any perturbations are referred to as baseline solutions. A validated code using a structured finite-volume discretization, nominally second-order accurate spatially was used for the simulations. Requisite grid independence studies were carried out for all cases.

The contoured nozzle geometries studied in this investigation are outlined in Figure 1. The ARN1 and the ARN2 are convergent nozzles with inlet diameters of 25.4 mm and 50.1 mm, respectively. The SMC000 nozzle has a inlet diameter of 50.8 mm. The Eggers Nozzle Eggers (1966) is a convergent-divergent contoured nozzle and was designed using the method of characteristics for $Ma = 2.22$ with an exit diameter of 26 mm.

3. Results and discussion

The first flow case corresponds to Set point 3 using the ARN1 design. The flow profiles are delineated at three locations $x/D_j = 4, 8, 12$, thus encompassing a broad swathe of the development region. As can be observed in Figure 2 there is a significant discrepancy between the PIV data and the baseline predictions of the $k-\omega$ SST model for the mean axial velocity profiles. The uncertainty bounds account for most of this discrepancy. Most of the experimental measurements lie inside the uncertainty bounds and even for data points not inside the envelope, the uncertainty in experimental measurements intersects the uncertainty bounds. In Figure 3, the corresponding bounds on the turbulent kinetic energy profiles are exhibited. Once again, the uncertainty bounds are able to account for a significant portion of the discrepancy, both near the nozzle exit and farther downstream.

The second flow case corresponds to Setpoint 7 using the ARN2 design. Figure 4 exhibits the relevant profiles and uncertainty bounds at select locations in the exhaust jet for the mean axial velocity profiles. Similar to Set point 3, the uncertainty bounds account for most of the predictive discrepancy. Furthermore, the uncertainty bounds capture the nature of the discrepancy: where the discrepancy is large, the uncertainty envelope is broad and where the discrepancy is small, the width of the uncertainty bounds is correspondingly small as well. This is encouraging as it suggests that the physics-based approach seems to account for not just the discrepancy, but the physics underlying the discrepancy as well. In Figure 5, the corresponding bounds on the turbulent kinetic energy profiles are exhibited for Set point 7. As can be seen, the uncertainty estimates account for a substantial portion of the discrepancy.

The third flow case corresponds to a heated, sub-sonic jet (Setpoint 23) using the Small Metal Chevron (SMC000) design. As can be seen in Figure 6, the uncertainty bounds

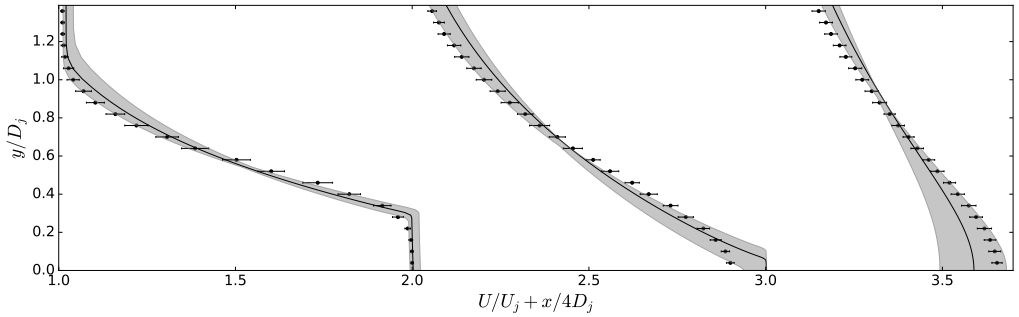

FIGURE 2. Mean axial velocity profiles in the nozzle jet exhaust for Set point 3. The dark lines represent the baseline predictions, the circles represent the PIV measurements of and the uncertainty bounds are shaded. The profiles are delineated at $x/D_j = 4$, $x/D_j = 8$, $x/D_j = 12$.

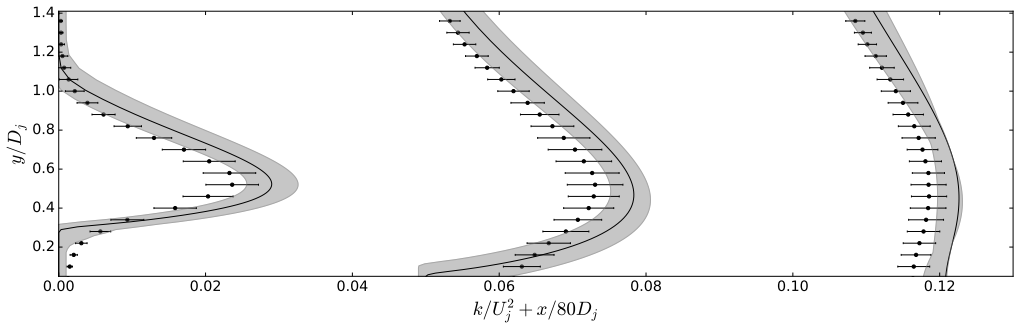

FIGURE 3. Turbulent kinetic energy profiles in the nozzle jet exhaust. The dark lines represent the baseline predictions, the circles represent the PIV measurements of and the uncertainty bounds are shaded. The profiles are delineated at $x/D_j = 4$, $x/D_j = 8$, $x/D_j = 12$.

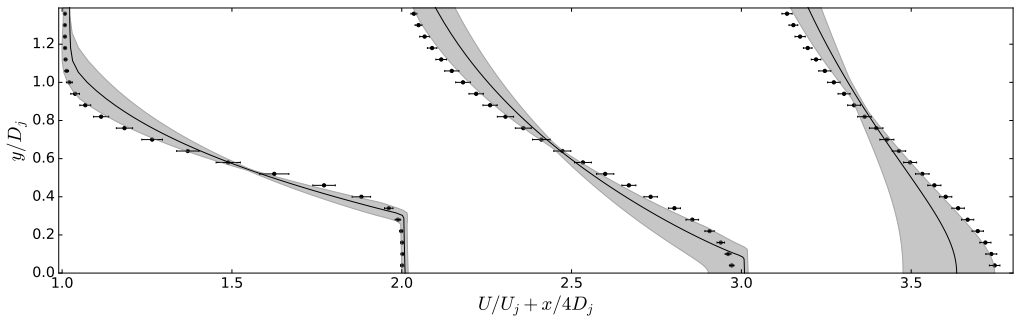

FIGURE 4. Mean axial velocity profiles in the nozzle jet for Setpoint 7, delineated at $x/D_j = 4, 8$ and 12.

account for almost all the discrepancy between RANS predictions and PIV data. Almost all the PIV data points lie inside the uncertainty envelope. In Figure 7, the corresponding bounds on the turbulent kinetic energy profiles are exhibited and account for most of the discrepancy.

Figure 8 exhibits the relevant profiles and uncertainty bounds at specific locations in the exhaust jet of (Eggers 1966). As can be observed in the figure, most data points are in the uncertainty estimate, which intersect the experimental error bounds at almost all

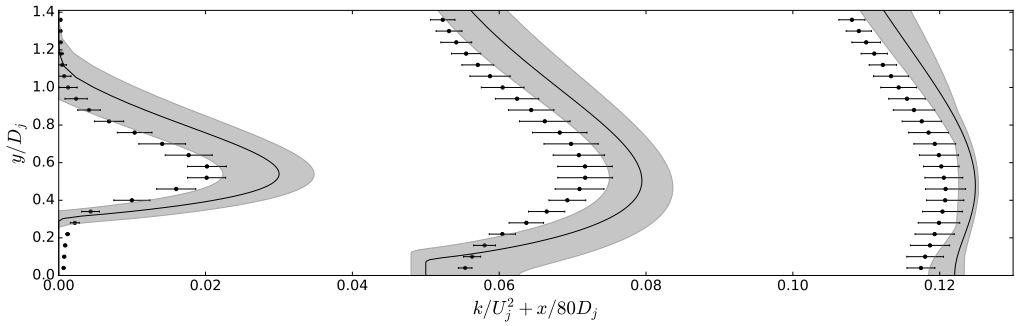

FIGURE 5. Turbulent kinetic energy profiles in the nozzle jet for Set point 7, delineated at $x/D_j = 4, 8$ and 12.

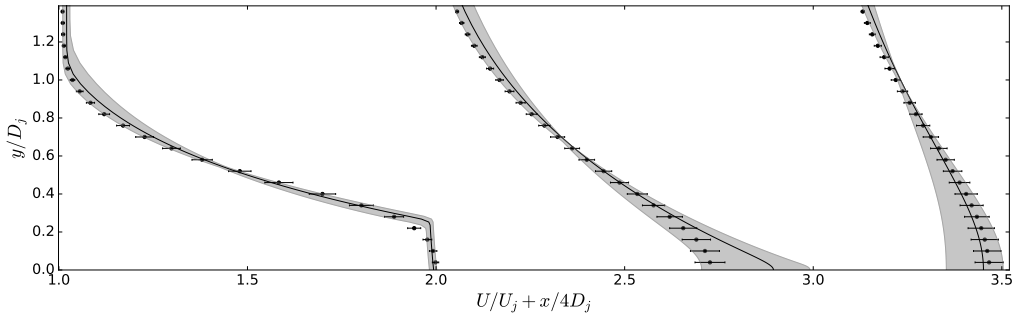

FIGURE 6. Mean axial velocity profiles in the nozzle jet for Set point 23, delineated at $x/D_j = 4, 8$ and 12.

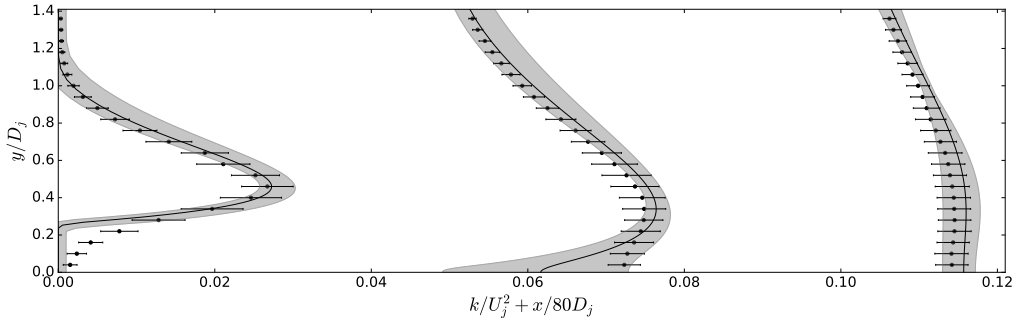

FIGURE 7. Turbulent kinetic energy profiles in the nozzle jet for Set point 23, delineated at $x/D_j = 4, 8$ and 12.

points. Very far downstream for instance at $x/D_j = 24$, where the discrepancy between predictions and measurements is considerably large, the uncertainty bounds still account for a significant portion of the discrepancy.

From the results, it is evident that the eigenspace perturbations lead to uncertainty ranges that can account for a significant proportion of the observed model inadequacy, under disparate flow conditions and for diverse Quantities of Interest. In the flow cases considered, this framework is able to exhibit uncertainty ranges that provide a prudent lower bound on the uncertainty in predictions and thus, may even be of utility in the

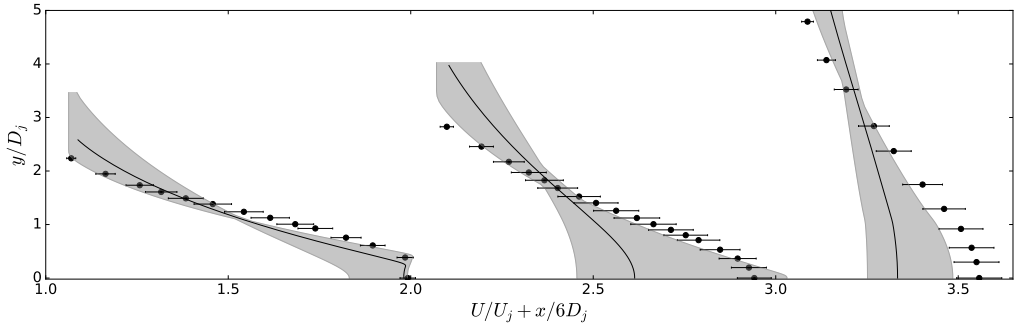

FIGURE 8. Mean axial velocity profiles in the nozzle jet exhaust for the Eggers experiment, delineated at $x/D_j = 6, 12$ and 24.

engineering design process. In a select few instances the experimental measurements remain beyond the predicted ranges. In this regard, it is important to outline that a modicum of the discrepancy is also due to assumptions made in the computations, such as the use of steady simulations to represent a potentially unsteady flow, etc.

4. Conclusion

The objective of this investigation is to exhibit the efficacy of the eigenspace perturbation methodology to account for the discrepancy between RANS predictions and high-fidelity measurements in turbulent jets exhausting from contoured nozzles. The investigation considered a variety of such turbulent jets: heated, cooled and isothermal; super- and sub-sonic; emanating from different nozzle geometries; focusing on varied Quantities of Interest, etc. In all cases, it was observed that the uncertainty estimates engendered via eigenspace perturbations were able to account for a substantially significant proportion of the predictive discrepancy. Additionally, the uncertainty bounds engendered herein are inexpensive to compute as they involve just five distinct RANS simulations. Furthermore, the results suggest that these bounds may be of potential engineering utility to guide design decisions for aerospace applications.

Acknowledgments

This work was supported by the DARPA under the Enabling Quantification of Uncertainty in Physical Systems (EQUiPS) project (technical monitor: Dr Fariba Fahroo).

REFERENCES

DEMBOWSKI, M. A. & GEORGIADIS, N. J. 2002 *An evaluation of parameters influencing jet mixing using the wind navier-stokes code*. NASA-TM-2002-211727.

EGGERS, J. 1966 *Velocity profiles and eddy viscosity distributions downstream of a mach 2.22 nozzle exhausting to quiescent air*. NASA-TN-D-3601.

EMORY, M., LARSSON, J. & IACCARINO, G. 2013 Modeling of structural uncertainties in Reynolds-averaged navier-stokes closures. *Phys. Fluids* **25**, 110822.

EMORY, M., PECNIK, R. & IACCARINO, G. 2011 Modeling structural uncertainties in reynolds-averaged computations of shock/boundary layer interactions. *AIAA J.* **479**, 1–16.

Engblom, W., Khavaran, A. & Bridges, J. 2004 Numerical prediction of chevron nozzle noise reduction using wind-mgbk methodology. *AIAA Paper* #2004-2979.

Georgiadis, N. J., Rumsey, C. L., Yoder, D. A. & Zaman, K. B. 2006*a* Turbulence modeling effects on calculation of lobed nozzle flowfields. *J. Propul. Power* **22**, 567–575.

Georgiadis, N. J., Yoder, D. A. & Engblom, W. B. 2006*b* Evaluation of modified two-equation turbulence models for jet flow predictions. *AIAA J.* **44**, 3107–3114.

Gorlé, C., Emory, M., Larson, J. & Iaccarino, G. 2012 Epistemic uncertainty quantification for rans modeling of the flow over a wavy wall. *Annual Research Briefs*, Center for Turbulence Research, Stanford University, pp. 81–91.

Hussein, H. J., Capp, S. P. & George, W. K. 1994 Velocity measurements in a high-reynolds-number, momentum-conserving, axisymmetric, turbulent jet. *J. Fluid M.* **258**, 31–75.

Iaccarino, G., Mishra, A. & Ghili, S. 2017 Eigenspace perturbations for uncertainty estimation of single-point turbulence closures. *Phys. Rev. Fluids* **2**, 024605.

Koch, L., Bridges, J. & Khavaran, A. 2002 Flow field comparisons from three Navier-Stokes solvers for an axisymmetric separate flow jet. *AIAA Paper* #2002-0672.

Menter, F. R. 1994 Two-equation eddy-viscosity turbulence models for engineering applications. *AIAA J.* **32**, 1598–1605.

Mishra, A. A. & Iaccarino, G. 2016 RANS predictions for high-speed flows using enveloping models. *Annual Research Briefs*, Center for Turbulence Research, Stanford University, pp. 289–301.

Mishra, A. A., Iaccarino, G. & Duraisamy, K. 2016 Epistemic uncertainty in statistical markovian turbulence models. *Annual Research Briefs*, Center for Turbulence Research, Stanford University, pp. 183–195.

Pope, S. 1978 An explanation of the turbulent round-jet/plane-jet anomaly. *AIAA J.* **16**, 279–281.

Sarkar, S., Erlebacher, G., Hussaini, M. & Kreiss, H. 1991 The analysis and modelling of dilatational terms in compressible turbulence. *J. Fluid Mech.* **227**, 473–493.

Schneider, W. 1985 Decay of momentum flux in submerged jets. *J. Fluid Mech.* **154**, 91–110.

Tam, W., Christopher, K. & Ganesan, A. 2004 Modified kappa-epsilon turbulence model for calculating hot jet mean flows and noise. *AIAA J.* **42**, 26–34.

Taulbee, D., Hussein, H. & Capp, S. 1987 The round jet-experiment and inferences on turbulence modeling. In *6th Symposium on Turbulent Shear Flows*, pp. 5–10.

Thies, A. T. & Tam, C. 1996 Computation of turbulent axisymmetric and nonaxisymmetric jet flows using the k-epsilon model. *AIAA J.* **34**, 309–316.

Wu, J., Wang, J. & Xiao, H. 2015 A bayesian calibration–prediction method for reducing model-form uncertainties with application in rans simulations. *Flow Turbul. Combust.* **73**, pp. 1–26.

Xiao, H., Wang, J. & Ghanem, R. G. 2016 A random matrix approach for quantifying model-form uncertainties in turbulence modeling. In arXiv preprint, arXiv:1603.09656.